Direct Measurements of Reynolds Stresses and Turbulence in the Bottom Boundary Layer

Joseph Katz
Department of Mechanical Engineering
The Johns Hopkins University, 3400 N. Charles Street
Baltimore, MD 21218
phone: (410) 516-5470 fax: (410) 516-7254 email: katz@titan.me.jhu.edu

Thomas Osborn
Department of Earth and Planetary Sciences
The Johns Hopkins University, 3400 N Charles Street
Baltimore, MD 21218-2681
phone (410) 516-7039 fax (410) 516-7933 email osborn@jhu.edu

Award Number: N000149510215

LONG-TERM GOALS

Predictions of the ocean dynamics, sediment transport, pollutant dispersal and biological processes require knowledge on the characteristics of turbulence in the bottom boundary layer. Modeling of the turbulence requires data for development/validation of closure models. Consequently our goal is to:

a. Measure the Reynolds stresses (free of wave contamination), velocity profile, dissipation rate, and turbulent spectra in the coastal bottom boundary layer using Particle Image Velocimetry (PIV).

b. Quantify the temporal variation of turbulent stresses, production, dissipation and buoyancy flux in relation to the oceanographic parameters that represent the local environment, such as waves, currents, stratification, internal waves and the nature of the water-sediment interface. The conclusions will quantify the relative importance of different mechanisms that control the flow and turbulence.

c. Study the mechanisms and extent of sediment re-suspension process by simultaneously measuring the flow structure and particle distributions.

d. Use oceanic PIV data for addressing Sub-Grid Scale Modeling issues for Large Eddy Simulation in oceanic flows.

e. Examine the structure of the flow, vertical vorticity transport, formation and upward migrations of large coherent vortex structures. Presently there is very little information on the dynamics and impact of large coherent structure in the bottom boundary layer on turbulence and sediment entrainment.

OBJECTIVES

Our effort for the past year focused on several objectives:

a. A field trip (funded in part by the present ONR grant and in part by NSF) to the vicinity of LEO-15 took place in the fall of 2001. We have used a new platform that has a profiling range that extends from very close to the bottom up to 10 m above the bottom.

Report Documentation Page

Form Approved
OMB No. 0704-0188

1. REPORT DATE	2. REPORT TYPE	3. DATES COVERED
SEP 2002		**00-00-2002 to 00-00-2002**

4. TITLE AND SUBTITLE	5a. CONTRACT NUMBER
Direct Measurements of Reynolds Stresses and Turbulence in the Bottom Boundary Layer	5b. GRANT NUMBER
	5c. PROGRAM ELEMENT NUMBER
6. AUTHOR(S)	5d. PROJECT NUMBER
	5e. TASK NUMBER
	5f. WORK UNIT NUMBER
7. PERFORMING ORGANIZATION NAME(S) AND ADDRESS(ES) **Department of Mechanical Engineering,,The Johns Hopkins University, 3400 N. Charles Street,,Baltimore,,MD, 21218**	8. PERFORMING ORGANIZATION REPORT NUMBER
9. SPONSORING/MONITORING AGENCY NAME(S) AND ADDRESS(ES)	10. SPONSOR/MONITOR'S ACRONYM(S)
	11. SPONSOR/MONITOR'S REPORT NUMBER(S)

12. DISTRIBUTION/AVAILABILITY STATEMENT
Approved for public release; distribution unlimited

13. SUPPLEMENTARY NOTES

14. ABSTRACT
Predictions of the ocean dynamics, sediment transport, pollutant dispersal and biological processes require knowledge on the characteristics of turbulence in the bottom boundary layer. Modeling of the turbulence requires data for development/validation of closure models.

15. SUBJECT TERMS

16. SECURITY CLASSIFICATION OF:			17. LIMITATION OF ABSTRACT	18. NUMBER OF PAGES	19a. NAME OF RESPONSIBLE PERSON
a. REPORT	b. ABSTRACT	c. THIS PAGE			
unclassified	**unclassified**	**unclassified**	**Same as Report (SAR)**	**9**	

b. Analysis of the PIV data obtained in several deployment, including data recorded in the near LEO–15 during summers 2000 and Fall 2001, and in the mouth of the Delaware Bay in 2000. In these experiments we recorded data in two sample areas simultaneously. The data has been used for:

1. Measuring the mean velocity distributions, RMS values of velocity fluctuations (free of wave contamination by using structure functions), turbulence energy spectra, dissipation rates, and the Taylor micro-scale Reynolds number. The results are used for characterizing the turbulence in the vicinity of LEO-15 under various conditions of mean current and wave amplitude.

2. Examining the flow structure, including the dynamics and distributions of large-scale vortices.

3. Measuring the Sub grid Scale (SGS) stresses needed for applications of Large eddy Simulations (LES) for modeling of oceanic turbulence. The results are then used for estimating the SGS energy flux (dissipation) and comparing it to the viscous dissipation rate. The SGS dissipation is a quantitative measure of energy transfer between turbulence at different length scales. Thus, its dynamics sheds light on the interaction between structures of different sizes.

4. Evaluating the performance of several, commonly used SGS stress models, including the Samgorinsky, Eddy Viscosity model, and the non-liner model.

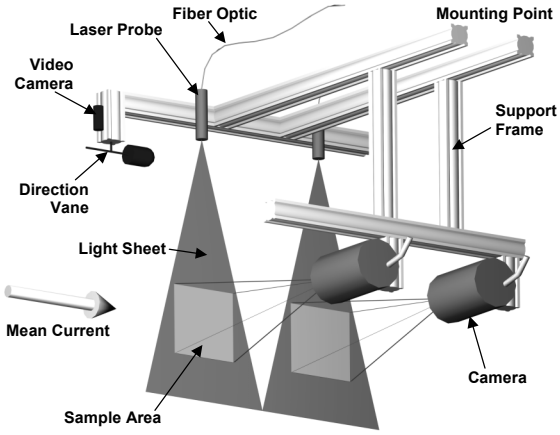

Figure 1. The oceanic PIV system.

APPROACH

The oceanic PIV system is described in refs. 12-13. The present system has improved substantially from the original setup described in refs. 2 & 4. A schematic of the submerged components is shown in Figure 1. The laser (a pulsed dye laser generating pairs of 2 μs pulses) is located on the ship and the light is transmitted through optical fibers to submerged probes. Images are acquired using two 2k x 2k CCD cameras, each with a maximum sampling rate of 4 frames/s. Each camera and associated light sheet can be aligned independently, in the same or different planes, near each other or apart. The data is recorded on mass data acquisition systems (one for each camera), allowing continuous sampling at 0.5 Hz for over 15Hrs. The data analysis procedures are described in refs. 12, 13, 17 and 18.

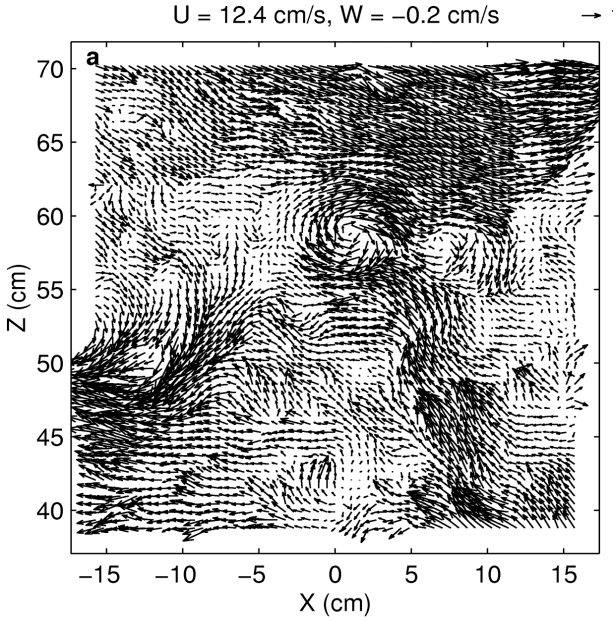

Figure 2. Velocity vector map. The area mean velocity is subtracted from each vector. The vertical coordinates represent the actual distance from the bottom.

Each instantaneous velocity distribution consists of 63x63 vectors, and the vector spacing, δ, is indicated in Table 1. A sample is presented in Figure 2.

The submersible components of the PIV system are mounted on a seabed platform, which can be rotated to align the sample areas with the mean flow direction, and extend vertically to sample at different elevations. The platform is a 5-stage telescopic hydraulic cylinder, with a vertical range of 9.75m. The system also contains a CTD, transmissometer, dissolved oxygen sensor, precision pressure transducer, clinometer, digital compass and video-microscope for sampling the particle distributions at high magnification.

WORK COMPLETED

In refs 12 & 13 we select and compare several data sets obtained at different depth to represent conditions of relatively high, intermediate and weak mean flows. They also represent substantially different turbulent Reynolds numbers. Table 1 summarizes the selected data series. To characterize the mean flow and amplitude of surface waves, we average the velocity over the vector map to obtain the instantaneous average velocity components (U and W). The mean current is characterized by $\overline{U}$ and $\overline{W}$, the overall average (over all distributions), whereas U_{RMS} and W_{RMS} are their RMS values, representing mostly the effect of surface waves but also turbulence at scales larger than the instantaneous distributions. The data of Runs A and B were obtained at the mouth of the Delaware Bay, at a mean near the bottom velocity of 38 cm/s with little wave motion. Runs C to F took place in Fall 2001 near LEO-15. The current in this region is moderate to weak, but it is exposed to oceanic swell. For Runs C and D the amplitude of the wave induced velocity is of the same magnitude as the mean flow. For Runs E and F, the mean current is very low, namely the flow consists almost entirely of wave induced motion. Data were collected continuously for periods of 20 min, at 2 - 3.3 Hz, and at elevations up to 8.5 m above the seabed. Here we use data obtained at mean elevations (vector map center) of 0.55 and about 2.5 m above the bottom.

Table 1. The selected data sets showing mean velocity, wave induced motion (U_{RMS}, W_{RMS}), RMS values of turbulent velocity fluctuations (u'. w'), Taylor microscale and resulting Re_{λ}^{u}.

Run	Site	frames	Elevationcm	$\overline{U}$ (cm/s)	U_{RMS} (cm/s)	$\overline{W}$ (cm/s)	W_{RMS} (cm/s)	u' (cm/s)	w' (cm/s)	λ^{u} (cm)	Re_{λ}^{u}
A	Del. Bay	900	144	38.2	2.8	-0.8	1.4	1.82	1.80	2.5	325
B	Del. Bay	900	35	32.6	3.7	-0.3	1.2	2.20	1.86	2.8	440
C	LEO-15	4000	257	14.9	4.5	-0.8	0.7	0.55	0.55	2.1	83
D	LEO-15	4000	55	7.7	3.3	-0.2	0.3	0.55	0.50	2.1	83
E	LEO-15	2400	245	-0.5	4.0	0.1	0.7	0.33	0.26	1,6	37
F	LEO-15	2400	55	0.9	3.2	-0.1	0.1	0.28	0.20	1.4	28

Figure 2 demonstrates the presence of large-scale vortical structures, which appear intermittently in all the data sets except for those with very low mean velocity (E and F). Figure 3 presents mean, one-dimensional energy spectra of u (E_{11}) and w (E_{33}) integrated along the streamwise (k_1) directions. These spectra do not involve use of the Taylor's Hypothesis. In addition, each graph contains an insert containing the distributions of $\varepsilon_{LF}^{-2/3} k_1^{5/3} E_{ii}(k_1)$ and $(3/4)\varepsilon_{LF}^{-2/3} k_1^{5/3} E_{ii}(k_1)$. As is evident, the turbulence is anisotropic at all scales. In most cases the vertical velocity spectra have a range of wavenumbers with a -5/3 slope, but the horizontal velocity spectra do not. The horizontal spectra appear to have 'bumps'. The magnitudes of these bumps are emphasized in the inserts that have a linear vertical axis. The existence of such bumps has been observed in previous measurements (e.g. refs. 19, 20, 3) and explained theoretically in refs. 5 & 10. They are attributed to a "bottleneck" that occurs at the transition between the inertial and dissipative range of the turbulence spectrum.

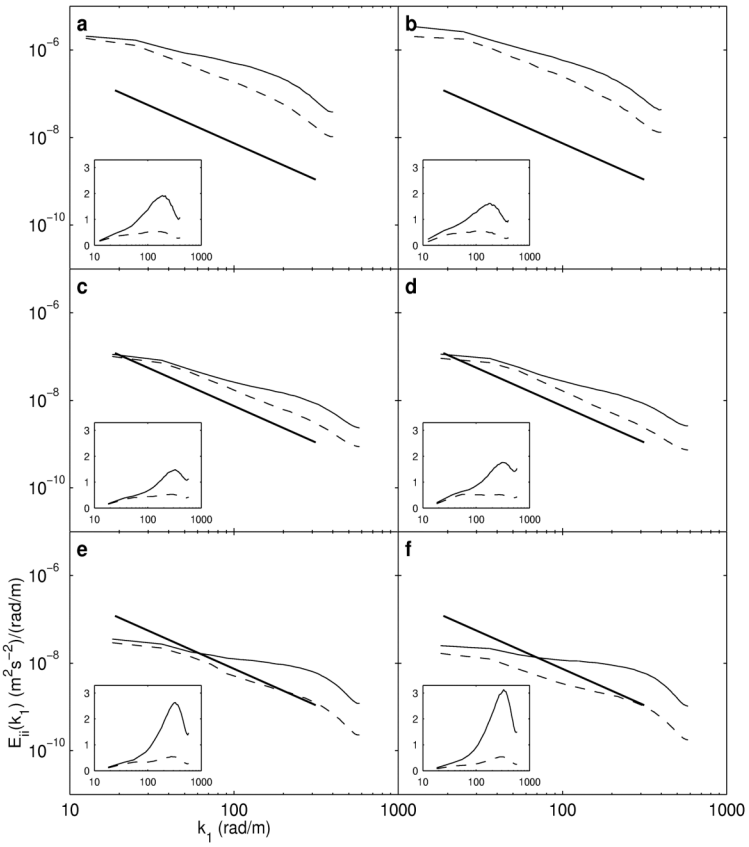

Figure 3. Mean spatial energy spectra. Solid lines: $E_{11}(k_1)$, Dashed lines: $3/4E_{33}(k_1)$. Inset figures are spectra of $\varepsilon_{LF}^{-2/3} k_1^{5/3} E_{ii}(k_1)$. a - f correspond to Runs A - F.

Since the spectra of the vertical velocity appear to have a more extended "inertial" range, we use $E_{33}(k_1)$ to estimate the dissipation rate, denoting this estimate as ε_{LF}. The results are summarized in Table 2. Having data that extends to wavenumbers in the dissipation range, enables us to obtain more "direct" estimate for the dissipation (ref. 4) using all or some of the measured velocity gradients.

$$\varepsilon_D = 3\nu\left[\left(\frac{\partial u}{\partial x}\right)^2 + \left(\frac{\partial w}{\partial z}\right)^2 + \left(\frac{\partial u}{\partial z}\right)^2 + \left(\frac{\partial w}{\partial x}\right)^2 + 2\left(\frac{\partial u}{\partial z}\frac{\partial w}{\partial x}\right) + \frac{2}{3}\left(\frac{\partial u}{\partial x}\frac{\partial w}{\partial z}\right)\right];\ \varepsilon_{\partial z} = \frac{15}{2}\nu\left(\frac{\partial u}{\partial z}\right)^2;\ \varepsilon_{\partial x} = \frac{15}{2}\nu\left(\frac{\partial w}{\partial x}\right)^2$$

Values are also presented in Table 2, along with the Kolmogorov scale, $\eta = (\nu^3/\overline{\varepsilon}_D)^{1/4}$.

Errors associated with the data being under resolved are in the 25%-45% range. There are significant spatial variations between Instantaneous distributions comparing ε_D, $\varepsilon_{\partial x}$ and $\varepsilon_{\partial z}$ of the same data show but when averaged, $\overline{\varepsilon_D}$ and $\overline{\varepsilon_{\partial z}}$ are consistently very close to each other (supporting the validity of results that would be obtained from vertical profiling), whereas $\overline{\varepsilon_{\partial x}}$ is consistently 55-64% smaller than $\overline{\varepsilon_D}$. The consistently lower values of $\overline{\varepsilon_{\partial x}}$ seem to be associated with the anisotropy of the oceanic turbulence. The trends of $\overline{\varepsilon_{LF}}$ differ significantly from the other methods and do not provide meaningful results for Runs C-F, the moderate and weak flows.

One can characterize the turbulence using the Taylor micro-scale Reynolds number, $\mathrm{Re}_\lambda^u \approx u'\lambda/\nu$, $\lambda^u \approx u'(15\nu/\bar{\varepsilon})^{1/2}$. To estimate $\overline{u}'$ and $\overline{w}'$ without being contaminated by waves one can use the second order structure function, a method introduced by Trowbridge (22), and implemented using PIV data in refs. 12 & 13. Averaged values of $\overline{u}'$ and $\overline{w}'$ and the corresponding Re_λ are also presented in Table 2. In Runs A and B Re_λ is in the 300-400 range, i.e. a "high" turbulence level. However, Re_λ of the LEO-15 site are 68-83 at moderate flow, and 14-27 when the mean current is weak. Since Runs C-F represent typical calm weather conditions near LEO–15, the results indicate that turbulence in the coastal bottom boundary layer in calm weather has a very low Reynolds number. The moderate and low Re_λ cases fall in the range where assumptions of universality of the energy spectrum are invalid (ref. 16).

Table 2. Dissipation rates, Kolmogorov Scale (η), vector spacing (δ) and SGS dissipation ($\bar{\varepsilon}_{SG}$).

Run	$\bar{\varepsilon}_{LF}$ x10^7 (m^2/s^3)	$\bar{\varepsilon}_D$ x10^7 (m^2/s^3)	η (mm)	δ (mm)	$\bar{\varepsilon}_{\partial x}$ x10^7 (m^2/s^3)	$\bar{\varepsilon}_{\partial z}$ x10^7 (m^2/s^3)	$\bar{\varepsilon}_{SG}(4\delta)$ x10^7 (m^2/s^3)	$\bar{\varepsilon}_{SG}(8\delta)$ x10^7 (m^2/s^3)	$\bar{\varepsilon}_{SG}(16\delta)$ x10^7 (m^2/s^3)	*Cs*
A	217	109	0.71	7.84	44.6	100	12.1	30.8	61.5	0.093-0.14
B	307	127	0.68	7.84	58.9	117	102	185	273	0.13-0.16
C	7.65	14.7	1.17	5.41	6.74	12.7	0.07	0.59	1.15	0.094-0.12
D	5.68	15.0	1.16	5.41	6.87	13.1	0.36	1.10	1.79	0.077-0.11
E	1.92	8.78	1.33	5.41	3.52	7.65	0.03	0.09	0.14	0.068-0.10
F	1.47	8.20	1.35	5.41	2.98	7.18	-0.05	-0.05	-0.05	fail

PIV data can also be used for evaluating models of the sub-grid scale (SGS) stresses, and for estimating the SGS dissipation (or energy flux) for Large Eddy Simulations (LES) (Liu et al., 1994). In LES the Navier Stokes Equations are filtered spatially at a scale Δ and the resulting SGS stresses, $\tau_{ij}^{SGS} = \widetilde{u_i u_j} - \tilde{u}_i \tilde{u}_j$ ("~" indicates spatial filtering) must be modelled (see example in Figure 4). Associated with this stress is the SGS dissipation rate, $\varepsilon^{SG} = -\tau_{ij}^{SGS}\tilde{S}_{ij}$, $\tilde{S}_{ij} = 0.5(\partial\tilde{u}_i/\partial x_j + \partial\tilde{u}_j/\partial x_i)$, which represents transfer of energy from the resolved to subgrid scales Consequently, attempts to model the SGS stresses frequently focus on reproducing the correct levels of ε^{SG}. Unlike viscous dissipation, ε^{SG} can be both positive and negative. A positive value indicates flux of energy from large to small scales whereas a negative value indicates "backscatter" of energy from small to large scales. Reviews are available in refs. 7, 11 and 14. When the filter is in the inertial range of isotropic, homogeneous turbulence, the mean ε^{SG} is (almost) equal to the viscous dissipation rate. However, ref. 15 show that near the wall of channel flows, the mean ε^{SG} is small and even negative.

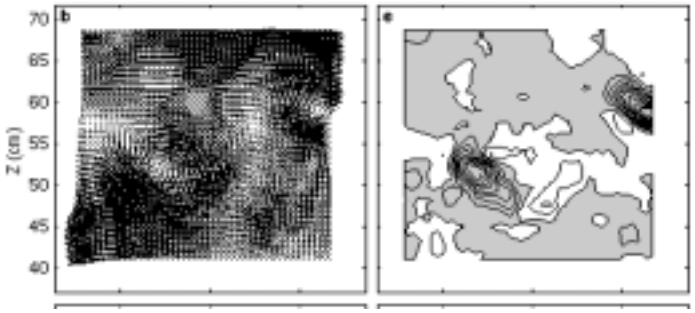

Figure 4. Instantaneous distributions of the velocity field shown in Figure 2 filtered at $\Delta=8\delta$ and the corresponding distributions of τ_{13}, contoured at intervals of $5x10^{-6}$ m^2/s^2. Negative values are shaded gray.

The Smagorinsky, eddy viscosity model (8, 21) for the SGS stress tensor is $\tau_{ij}^S = -2(c_S\Delta)^2|\tilde{S}|\tilde{S}_{ij}$, where $|\tilde{S}| = \sqrt{2\tilde{S}_{ij}\tilde{S}_{ij}}$, Δ is the filter scale, and c_S is a coefficient that has to be determined. The coefficient is calculated by matching the measured and modelled ε^{SG}, using (12)

$$\varepsilon^{SG} = -\tau_{ij}\tilde{S}_{ij} \approx -\frac{1}{2}\left(\tau_{11}\tilde{S}_{11} + \tau_{33}\tilde{S}_{33} - \tau_{11}\tilde{S}_{33} - \tau_{33}\tilde{S}_{11} + 12\tau_{13}\tilde{S}_{13}\right)$$

We also estimate the coefficients of the non-linear model (refs. 1, 6).

Measured averaged values of ε^{SG} are presented in Table 2 for three filter sizes, Δ=4, 8 and 16 vector spacings (δ, Table 1). At high flow (A-B) $\overline{\varepsilon^{SG}}$ is of the same order as $\overline{\varepsilon_D}$, whereas in the moderate and weak mean flow conditions, the SGS dissipation is more than an order of magnitude lower than $\overline{\varepsilon_D}$, decreasing to negligible levels as the flow diminishes. Considering that cases C-F represent typical calm weather conditions near LEO 15, the results bear significant implications for applications of LES to coastal flows. Ref. 12 contains a discussion on differences between positive and negative energy fluxes and correlations between modeled and measured SGS stresses. The Smagorinsky model coefficients (Table 2) decrease with decreasing mean flow rate, and cannot be determined for run F, due to a negative $\overline{\varepsilon^{SG}}$. The non-linear model coefficients are meaning less due to the low $\overline{\varepsilon^{SG}}$.

IMPACT

The present measurements and analysis enable us to characterize the flow structure and turbulence in the bottom boundary layer of the coastal ocean in great detail. The measurements provide distributions of Reynolds stresses, spectra, dissipation rate, characteristics of SGS stresses and energy transfer across scales, all free of contamination by surface waves. These data are essential for modeling of coastal circulation, sediment and pollutant transport, and biological processes.

TRANSITIONS

During FY 2000 & 2001 the submersible PIV system has been used extensively at NSWC/Carderock to measure the flow structure within wakes behind several maneuvering models.

RELATED PROJECTS

The research involving measurements of flow structure and turbulence in the coastal ocean using PIV has been funded in part by ONR (present project) and in part by NSF (9871961). The NSF sponsored

project focuses with the flow/turbulence in the water column above the boundary layer, whereas the present project focuses on the boundary layer.

REFERENCES

1. Bardina, J., J.H. Ferziger, and W.C. Reynolds, 1980: Improved subgrid scale models for large eddy simulation. *AIAA paper* No. 80–1357.

2. Bertuccioli, L., G. I. Roth, J. Katz, and T. R. Osborn, 1999: A submersible Particle Image Velocimetry system for turbulence measurements in the bottom boundary layer. *J. Atmos. Oceanic Technol.*, **16,** 1635-1646.

3. Champagne, F.H., C.A. Friehe, J.C. La Rue, and J.C. Wyngaard, 1977: Flux measurements, flux estimation techniques and fine scale turbulence measurements in the surface layer over land. *J. Atmos. Sci*., **34**, 515-530.

4. Doron, P., L. L. Bertuccioli, J. Katz, and T. R. Osborn, 2001: Turbulence characteristics and dissipation estimates in the coastal ocean bottom boundary layer from PIV data. *J. Phys. Oceanogr.*, **31**, 2108-2134.

5. Falkovich, G., 1994: Bottleneck phenomenon in developed turbulence. *Phys. Fluids,* **6,** 1411-1414.

6. Leonard, A., 1974: Energy cascade in large-eddy simulations of turbulent fluid flows. *Adv. Geophys*. **18**, 237.

7. Lesieur, M., and O. Metais, 1996: New trends in large-eddy simulations of turbulence. *Annu. Rev. Fluid Mech.*, **28**, 45–82.

8. Lilly, D.K., 1967: The representation of small-scale turbulence in numerical simulation experiments. *Proc. IBM Scientific Computing Symposium on Environmental Sciences*, 195.

9. Liu, S., C. Meneveau, and J. Katz, 1994: On the properties of similarity subgrid-scale models as deduced from measurements in a turbulent jet. *J. Fluid Mech.*, **275**, 83-119.

10. Lohse, D. and A Muller-Groeling, 1995: Bottleneck effects in turbulence: Scaling phenomena in *r* versus *p* space. *Phys. Rev. Lett.,* **74,** 1747-1750.

11. Meneveau, C., and J. Katz, 2001: Scale-invariance and turbulence models for large-eddy simulation, *Annu. Rev. Fluid Mech.*, **32**, 1-32.

12. Nimmo Smith, W. A. M., J. Katz, and T. R. Osborn, 2002b: On the Structure of Turbulence and Dynamics of subgrid-Scale Stresses in the Bottom Boundary Layer of the Coastal Ocean, *J. Phys. Oceanog,* submitted for publication.

13. Nimmo Smith, W. A. M., P. Atsavapranee, J. Katz, and T. R. Osborn, 2002a: PIV Measurements in the bottom boundary layer of the coastal ocean. *Exp. Fluids,* in press.

14. Piomelli, U., 1999: Large-eddy simulation: achievements and challenges. *Prog. Aerosp. Sci.*, **35**, 335.

15. Piomelli, U., Cabot, W. H., Moin, P. and S. Lee, (1991), "Subgrid-scale backscatter in turbulent and transitional flows," Phys. Fluids A 3, 1766.

16. Pope, S.B., 2000: *Turbulent Flows*, Cambridge University Press, 771 pp.

17. Roth, G. I., and J. Katz, 2001: Five techniques for increasing the speed and accuracy of PIV interrogation. *Meas. Sci. Technol.,* **16,** 1568-1579.

18. Roth, G. I., D. T. Mascenik, and J. Katz, 1999: Measurements of the flow structure and turbulence within a ship bow wave. *Phys. Fluids,* **11,** 3512-3523.

19. Saddoughi, S.G., 1997: Local isotropy in complex turbulent boundary layers at high Reynolds numbers. *J. Fluid Mech.*, **348,** 201-245.

20. Saddoughi, S.G., and S.V. Veeravalli, 1994: Local isotropy in turbulent boundary layers at high Reynolds numbers. *J. Fluid Mech.*, **268,** 333-372.

21. Smagorinsky, J., 1963: General circulation experiments with the primitive equations. I. The basic experiment. *Mon. Weather Rev*., **91**, 99.

22. Trowbridge, J.H., (1998), On a technique for measurement of turbulent shear stress in the presence of surface waves*," J. Atmos. Oceanic Technol.*, 15, 290-298.

PUBLICATIONS

1. Nimmo Smith, W. A. M., P. Atsavapranee, J. Katz, and T. R. Osborn, 2002a: PIV Measurements in the bottom boundary layer of the coastal ocean. *Exp. Fluids,* in press.

2. Nimmo Smith, W. A. M., J. Katz, and T. R. Osborn, 2002b: On the Structure of Turbulence and Dynamics of subgrid-Scale Stresses in the Bottom Boundary Layer of the Coastal Ocean, *J. Phys. Oceanog,* submitted for publication.